Three-dimensional structure of rat acid phosphatase

Gunter Schneider, Ylva Lindqvist and
Pirkko Vihko[1]

Department of Molecular Biology, Swedish University of Agricultural
Sciences, Uppsala Biomedical Center, Box 590, S-751 24 Uppsala,
Sweden and [1]Biocenter and Department of Clinical Chemistry,
University of Oulu, SF-90220 Oulu, Finland

Communicated by C.-I.Brändén

The crystal structure of recombinant rat prostatic acid
phosphatase was determined to 3 Å resolution with
protein crystallographic methods. The enzyme subunit
is built up of two domains, an α/β domain consisting of
a seven-stranded mixed β-sheet with helices on both sides
of the sheet and a smaller α domain. Two disulfide
bridges between residues 129–340 and 315–319 were
found. Electron density at two of the glycosylation sites
for parts of the carbohydrate moieties was observed. The
dimer of acid phosphatase is formed through two-fold
interactions of edge strand 3 from one subunit with strand
3 from the second subunit, thus extending the β-sheet
from seven to 14 strands. Other subunit–subunit inter-
actions involve conserved residues from loops between
helices and β-strands. The fold of the α/β domain is
similar to the fold observed in phosphoglycerate mutase.
The active site is at the carboxy end of the parallel strands
of the α/β domain. There is a strong residual electron
density at the phosphate binding site which probably
represents a bound chloride ion. Biochemical properties
and results from site-directed mutagenesis experiments
of acid phosphatase are correlated to the three-
dimensional structure.
Key words: crystal structure/prostatic acid phosphatase/
protein crystallography

Introduction

Acid phosphatases [orthophosphoric monoester phospho-
hydrolase (acid optimum)] catalyse the hydrolysis of
phosphate monoesters and in some cases, phosphoryl transfer
between a phosphoester and alcohols (for reviews see
Bodansky, 1972; van Etten, 1982; Vincent *et al.*, 1992).
Acid phosphatases are widely distributed in both the animal
and plant kingdoms and they can be divided into three
different types (Vincent *et al.*, 1992). Two such types are
the low molecular weight phosphatases of $\sim 18-20$ kDa as
found in human or bovine liver and the high molecular
weight phosphatases (45–60 kDa per subunit) such as the
enzymes from wheat germ, lysosomes and prostate. A third
class are the purple acid phosphatases which contain a
binuclear iron centre.

High molecular weight acid phosphatases (EC 3.1.3.2)
include enzymes with great differences in tissue localization,
substrate specificity, inhibition pattern and regulation. One

of the most studied enzymes in this class is the enzyme
synthesized under androgen induction in the prostate.
Prostatic acid phosphatase is synthesized with a 32 amino
acid leader sequence that directs the nascent chain to the
endoplasmic reticulum (Vihko *et al.*, 1988; Roiko *et al.*,
1990). The enzyme is secreted into the spermatic fluid,
where the mature, cleaved and N-glycosylated 354 residue
protein is found in very high concentrations (> 1 mg/ml)
(Rönnberg *et al.*, 1981). The enzyme is of considerable
medical interest, since prostatic acid phosphatase has been
used as a marker for prostatic cancer for a number of
decades. Development of metastatic prostatic cancer can be
monitored by the increase in the acid phosphatase concen-
tration in serum (Bodansky, 1972; Vihko *et al.*, 1981).

For most acid phosphatases, the natural substrate and the
biological role of the enzyme have yet to be established. In
general, acid phosphatases are rather non-specific with
respect to artificial substrates and can hydrolyse a broad
variety of phosphoesters, amongst them phosphotyrosine
(Lin and Clinton, 1986). As opposed to alkaline phos-
phatases, acid phosphatases (with the exception of purple
acid phosphatases) do not utilize metal ions for catalysis.
It has been suggested, based on biochemical evidence, that
the high molecular weight acid phosphatases are histidine
phosphatases, e.g. a phosphorylated histidine has been
proposed as an intermediate in enzyme-catalysed phospho-
ester hydrolysis (van Etten, 1982).

Here, we describe the three-dimensional structure of acid
phosphatase from rat prostate as a representative enzyme
of the high molecular weight type acid phosphatases.
Comparison of the enzyme subunit structure reveals no
similarity to the structure of alkaline phosphatase (Sowadski
et al., 1985). However, the topology of one of the domains
of acid phosphatase is similar to the structure of phospho-
glycerate mutase (Campbell *et al.*, 1974). We also correlate
the three-dimensional structure of acid phosphatase with
biochemical and site-directed mutagenesis data.

Results and discussion

Electron density map and quality of the model

Despite the rather low resolution of the electron density
map (3 Å), the electron density for both main chain and
side chains is very well defined (Figure 1). Except for the
last eight residues, which presumably are flexible, and
some side chains at the surface of the molecule, there is
continuous well defined electron density for the whole
polypeptide chain. Residue by residue real space correlation
(Brändén and Jones, 1990; Jones *et al.*, 1991) (average value
0.72) and other conventional criteria such as crystallographic
R-factor (20.4%), good stereochemistry of the model (bond
length r.m.s. of 0.021 Å), Ramachandran plot (very few
outliers from the allowed regions except glycine residues)
and the observed hydrogen bonding pattern all indicate that
the chain tracing for acid phosphatase is correct. This is
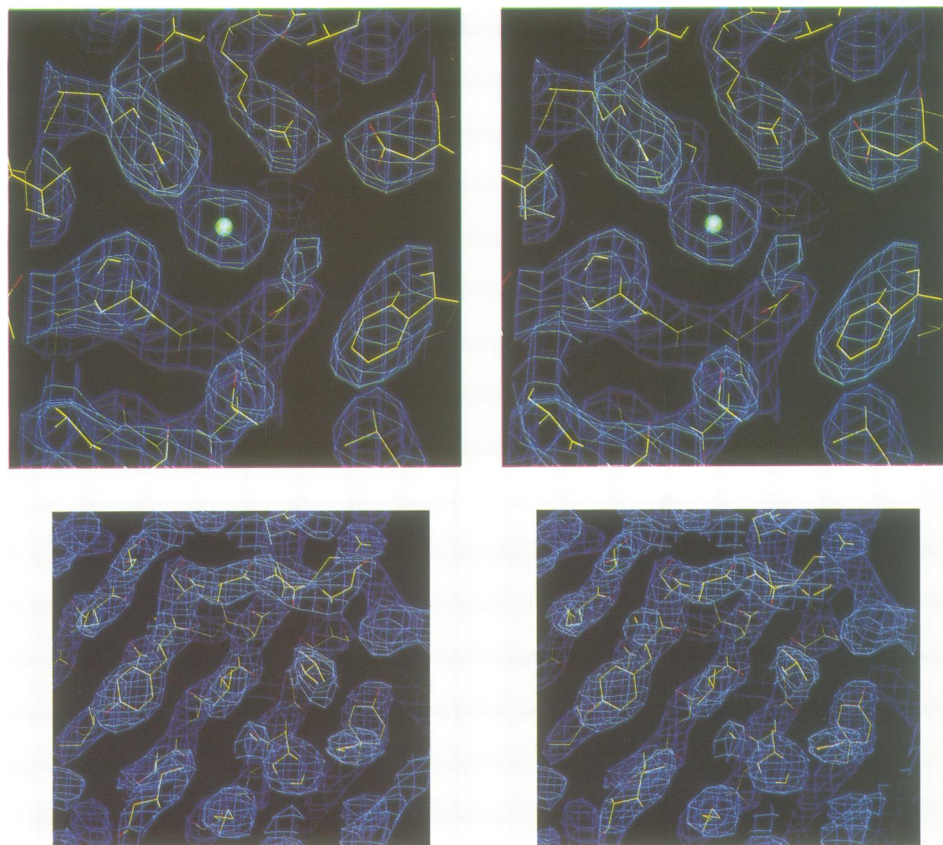
Fig. 1. Parts of the final $2|F_o| - |F_c|$ electron density for rat prostatic acid phosphatase. The contour level is at 1.5 times the standard deviation of the map. (**a**) View of the active site with the residual electron density close to the side chain of the conserved His12 which corresponds to a bound chloride ion shown as a green sphere; (**b**) part of the central core of the α/β domain.

also supported by the correlation of the three-dimensional structure with biochemical and site-directed mutagenesis data as discussed below. The present model of rat prostatic acid phosphatase consists of a protein chain comprising amino acid residues 1−342, a chloride ion and two carbohydrate moieties, one consisting of two N-acetylglucosamine and one mannose molecule and the second consisting of one N-acetylglucosamine molecule.

Overall structure

The subunit. The subunit is built up from two domains, an α/β domain and an α-helical domain (Figure 2). The α/β domain consists of a mixed β-sheet consisting of seven strands, with strand order 3, 2, 4 and 1 in parallel and strands 5, 6 and 7 in antiparallel conformation. The seventh strand is interrupted by a loop in the middle of the strand. The third and the two pieces of the seventh strand, i.e. the edge strands, are very short. There are α-helices on both sides of the sheet.

The smaller domain is not consecutive, but consists of very long excursions of the chain between strand 1 and helix 1 (residues 16−37) and between strand 3 and helix 9 (residues 115−227) in the α/β domain. The first segment of this chain is a long loop of irregular structure and the only secondary structure elements in the small domain are six α-helices, numbers 3, 4, 5, 6, 7 and 8 in the second chain excursion (Figure 2). This domain is located on top of the β-sheet of the α/β domain at the C-terminal end of the parallel β-strands. This topology gives the subunit the overall

shape of a flat disc, with approximate dimensions $30 \times 46 \times 62$ Å.

Three disulfide bridges had been proposed for human acid phosphatase (van Etten *et al.*, 1991). In the three-dimensional structure of the rat enzyme, only two of these disulfide bridges are found. One of these, residues 129−340, links the N-terminus of helix 3 to the C-terminus of the subunit. The second, between residues 315 and 319, is part of the looped-out structure in strand 7. The third disulfide, which had been proposed between residues 183 and 281, cannot be formed in the rat enzyme. Residues 183 and 281 are far from each other both in the subunit and in the dimer. Residue 183 is found in helix 6 in the small domain and residue 281 is part of the β-sheet as the first residue of strand 5. Another piece of evidence that these cysteine residues are not involved in a disulfide bridge is the fact that they provide the binding sites for the two mercury ions in the crystals of the heavy atom derivative obtained with $Hg(CH_3CO_2)_2$. Given the high homology between rat and human acid phosphatase, this disulfide bridge will not be present in the human enzyme either.

The dimer. The dimer (Figure 3) is formed through two-fold interactions between β-strand 3 of each subunit so that these two strands become antiparallel to each other, extending the seven-stranded sheet in the monomer to a 14-stranded β-sheet in the dimer. Also part of the dimer interface are residues from helices 1 and 2, and the loops between β-strand 1 to helix 1, helix 1 to β-strand 2 and helix 2 to β-strand 3.

Amongst the subunit−subunit interactions are, besides a
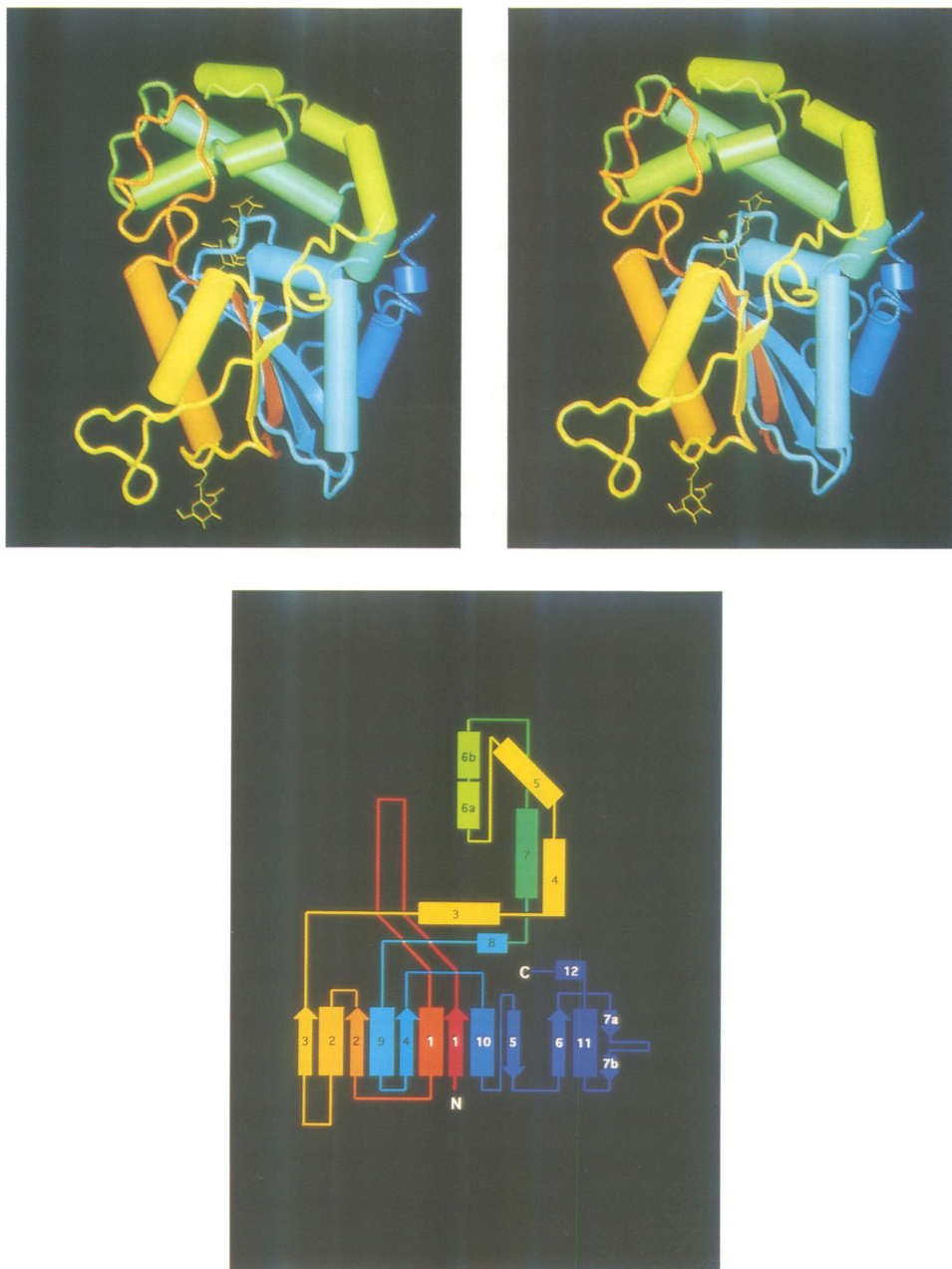
**Fig. 2.** Subunit structure of rat prostatic acid phosphatase. (**a**) Schematic view of the subunit. The molecule is colour coded according to sequence number, i.e. from red at the N terminus to blue at the C terminus. The disulfide bridges are shown in yellow, and the location of the active site is indicated by the position of the bound chloride ion (green sphere). The carbohydrate moieties are also included. (**b**) Folding diagram of acid phosphatase. Limits of secondary structural elements are $\beta1$, 3−11; $\alpha1$, 40−61; $\beta2$, 70−74; $\alpha2$, 78−91; $\beta3$, 112−114; $\alpha3$, 130−141; $\alpha4$, 143−149; $\alpha5$, 153−163; $\alpha6a$, 170−176; $\alpha6b$, 178−186; $\alpha7$, 197−215; $\alpha8$, 220−226; $\alpha9$, 228−243; $\beta4$, 251−256; $\alpha10$, 258−268; $\beta5$, 281−289; $\beta6$, 292−300; $\beta7a$, 308−310; $\beta7b$, 319−321; $\alpha11$, 321−328; $\alpha12$, 336−339.

number of hydrophobic contacts, possible hydrogen bonds between side chain atoms of residues Gln37 and His67, Tyr65 and Asp78 and Asp76 and His112. The side chains of residue Trp106 are stacked on top of each other across the two-fold axis relating the two subunits (Figure 3). All these interactions are conserved in lysosomal and prostatic acid phosphatases with the exception of His67. In lysosomal phosphatases, His67 is replaced by an arginine residue which can still interact with the glutamine side chain.

Comparison with phosphoglycerate mutase. The topology of the α/β domain of acid phosphatase shows considerable similarity to the fold of yeast phosphoglycerate mutase

(Campbell *et al.*, 1974). A superposition of the two domains gave an r.m.s. fit of 1.75 Å for 98 equivalent Cα atoms (Figure 4). This alignment also superimposes the sequence motif Arg, His, Gly, and a conserved His residue, spaced ∼170 residues apart in the mutase amino acid sequence, which are part of one of the phosphate binding sites in phosphoglycerate mutase (Winn *et al.*, 1981) with the corresponding conserved sequence motif and conserved His residue in acid phosphatase, here spaced ∼250 amino acids apart. As will be discussed below, this sequence motif is also involved in the binding of the phosphate group in acid phosphatases. In fact, the occurrence of this sequence motif in phosphoglycerate mutase, the bifunctional enzyme
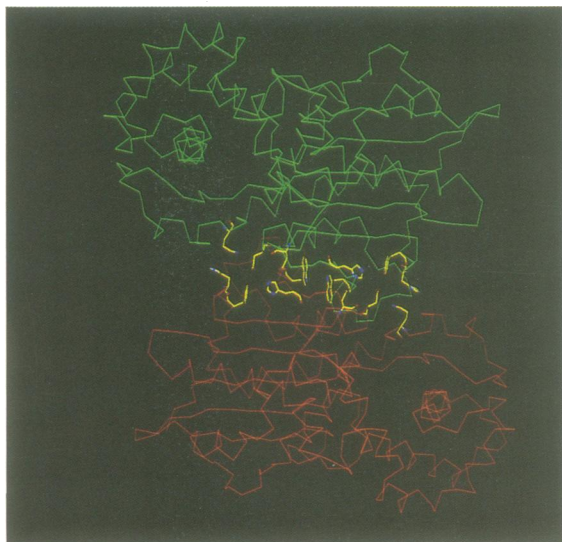
Fig. 3. The dimer of acid phosphatase. The two subunits are colour coded differently. The side chains of conserved amino acid residues at the interface are included.
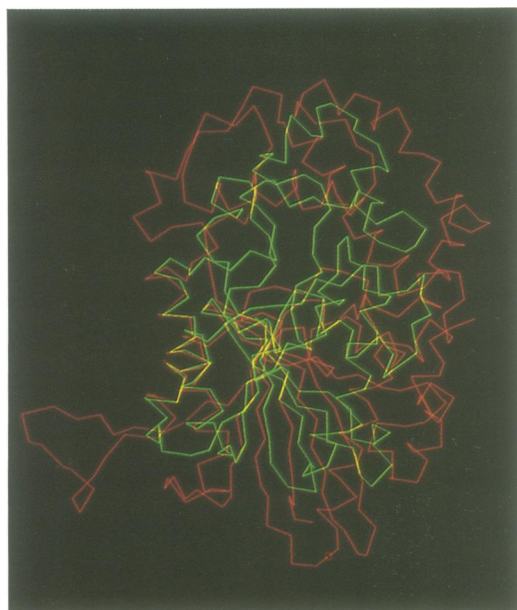
Fig. 4. Superposition of acid phosphatase (red) with phosphoglycerate mutase (green).

6-phosphofructo-2-kinase/fructose-2,6-bisphosphatase and in acid phosphatases led to the suggestion of a common fold for these three enzymes (Bazan *et al.*, 1989).

Glycosylation sites

Human prostatic acid phosphatase contains three N-linked glycosylation sites (Morris *et al.*, 1989) and the structures of the carbohydrate moieties have been elucidated by ^{1}H NMR spectroscopy (Risley and van Etten, 1987). No information on the status of glycosylation of native rat acid phosphatase is available but the corresponding asparagine residues 62, 188 and 301 are all conserved. All these asparagine residues are found in sequence motifs Asn-X-Thr/Ser, typical for possible glycosylation sites.

In our electron density maps, we find electron density extending from the side chains of residues Asn62 and Asn301 at the surface of the protein into the surrounding solution. The electron density at position Asn62 can be fitted to an *N*-acetylglucosamine molecule. At the glycosylation site at Asn301, it is possible to model the first three residues of one of the carbohydrate chains of the human enzyme, two *N*-acetylglucosamine sugars and one mannose into this electron density. The first *N*-acetylglucosamine sugar ring is stacked with the side chain of residue Tyr308 and makes polar interactions with the side chains of residues Asn272 and Glu302 (Figure 5). No indications for the third glycosylation site are found in the electron density map. However, this observation does not exclude the possibility that in native rat prostatic acid phosphatase, analogous to the human enzyme, three glycosylation sites are present. The additional carbohydrates at this site might be disordered in the crystals or the asparagine might not be glycosylated in the Sf9 cells used to produce the recombinant enzyme.

Active site

The active site is found at the carboxy end of the parallel β-strands of the α/β domain in the cleft between the two domains. The active sites are far apart (~ 34 Å) in the dimer and are not in direct contact with each other. The active site cleft is rather open and easily accessible from the outer solution (Figure 6). In fact there is an almost continuous solvent channel between the two domains right through the enzyme in the active site. Most of the active site residues come from the loops after strands 1 and 4. Residues Arg11, His12 and Arg15 are part of a sequence motif RHGXRXP characteristic for acid phosphatases (van Etten *et al.*, 1991). These residues are part of a cluster of conserved amino acid residues in the centre of the active site, consisting of residues Arg11, His12, Arg15, Arg79, His257 and Asp258.

All these residues are close to each other in space and form the phosphate binding site. His12 had previously been suggested as the residue which during catalysis forms the phosphohistidine intermediate (Ostanin *et al.*, 1992). In the close vicinity of the side chain of His12, there are the side chains of Arg11, Arg15, Arg79 and His257. These positively charged side chains form a pocket at the active site of a suitable size for a phosphate ion.

In all the electron density maps, there is strong spherical electron density close to the side chain of His12 (Figure 1) which is of too high a level to represent a bound water molecule. We interpret this electron density as an anion which is bound at the phosphate binding site. In the purification protocol, neither sulfate nor phosphate salts are used. It is therefore unlikely that this electron density represents a sulfate or phosphate ion. Furthermore, placing such an anion in the centre of this spherical density would position one of the oxygens much too close to the side chain of His12. Given the instability at acidic pH of the phosphorylated histidine intermediate (van Etten, 1982), it is also unlikely that the electron density represents such a trapped intermediate. One of the last steps of the purification procedure consists of a gel filtration in the presence of a high concentration of NaCl (0.15 M) (Vihko *et al.*, 1993). We therefore interpret this density as a chloride ion, bound at the phosphate binding site of the enzyme. This is in agreement with observations that small monovalent anions are weak inhibitors of the acid phosphatases (Yam, 1974). The unusual clustering of positive charges (three arginine
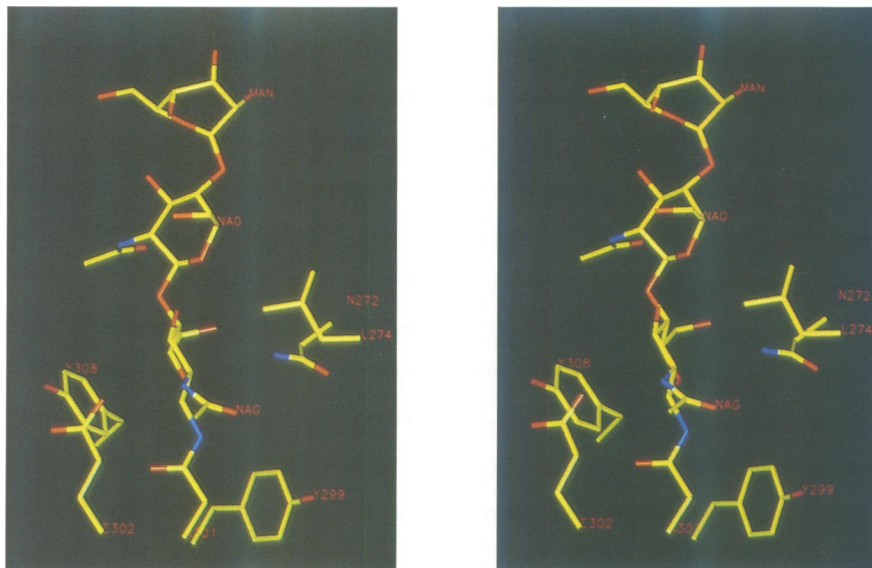
Fig. 5. Stereo view of the glycosylation site at Asn301 in prostatic acid phosphatase.
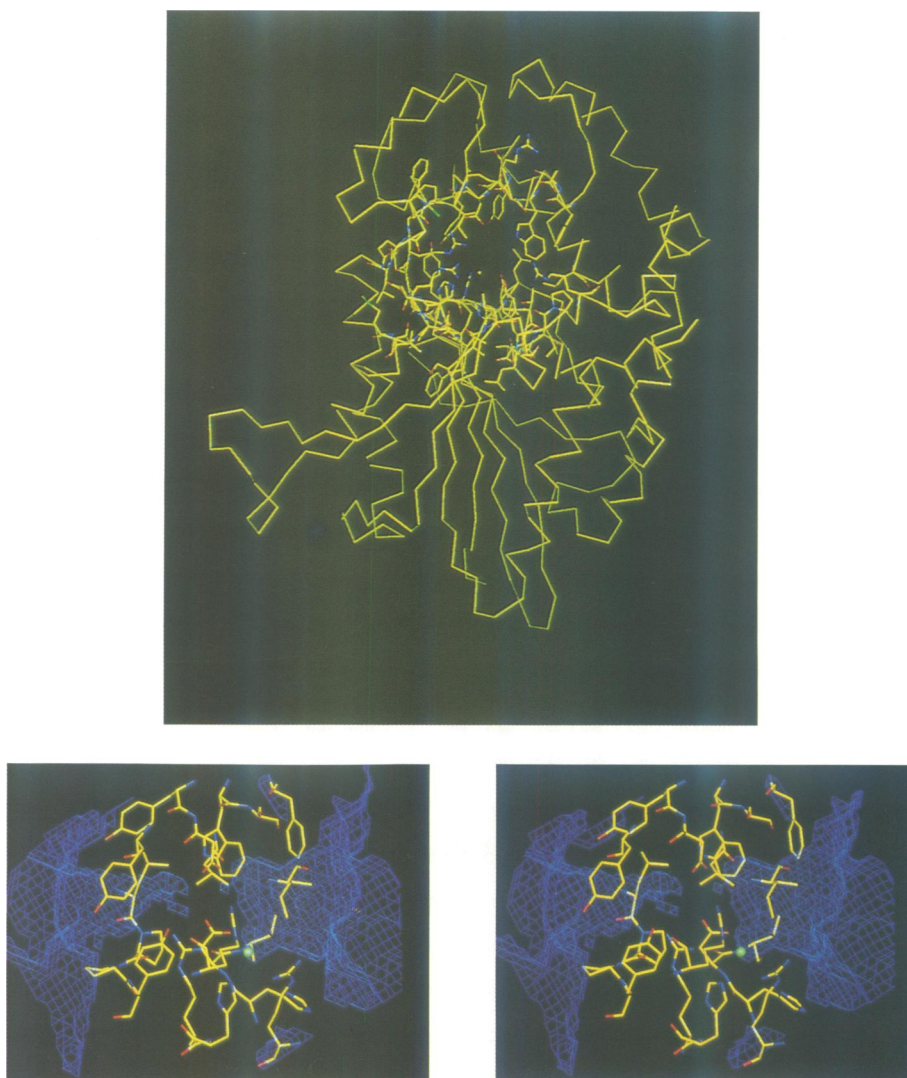

Fig. 6. (a) View of acid phosphatase illustrating the active site. Side chains within a 10 Å radius of the bond anion at the active site are shown. Note that there is an almost complete solvent channel through the molecule. (b) The surface of the accessible pocket at the active site of rat prostatic acid phosphatase. Calculated using a 1 Å probe with the program Voidoo, written by G.Kleiywegt.

and two histidine residues within <5 Å from the anion) must make this site an effective trap for negatively charged ions.

The conserved residues Arg11, His12, Arg15 and Arg79 thus form the phosphate binding site and residue His12 will become phosphorylated during catalysis. In the close vicinity of this binding site, there are also the conserved residues His257 and Asp258. The location of both these residues is such that they would be suitable candidates to act as acid/base catalysts during phosphoester hydrolysis. This question is presently being addressed by site-directed mutagenesis.

In the active site, many other residues that are conserved amongst prostatic and lysosomal acid phosphatases are found. To these belong the hydrophobic residues Trp174 and Tyr278; polar residues Thr80 and Thr259 which both interact with His257, and charged Asp179 which makes an ionic bond to Arg15.

Other conserved amino acid residues from the second domain, among them Cys183, are found in the cleft between the domains and might participate in substrate binding and/or catalysis. In the structure of the enzyme described here, they are too remote to participate directly in catalysis. It is, however, conceivable that part of this domain will move upon substrate binding; especially the irregular loop comprising residues 17−37 might fold back and in this way close off the active site after substrate binding. Such a conformational change could bring some residues closer to the catalytic centre.

Recently, some of the conserved residues of acid phosphatases have been the target for side chain replacements by site-directed mutagenesis of the *Escherichia coli* enzyme. Residues Arg16 and His17 (corresponding to Arg11 and His12 in rat prostatic acid phosphatase) have been shown to have critical roles in catalysis, since replacement of Arg16 by alanine and His17 by asparagine results in complete elimination of phosphatase activity (Ostanin *et al.*, 1992). These results are compatible with the X-ray structure, since both residues are located at the active site. His17 had been suggested to form the phosphorylated intermediate which is supported by X-ray analysis. Arg16 is part of the phosphate binding site. Replacement of residues Arg20, Arg87 and His303 (Arg15, Arg79 and His257 in rat prostatic acid phosphatase) by alanine results in mutant enzymes with phosphatase activities <0.4% of the wild-type enzyme (Ostanin *et al.*, 1992). In the X-ray structure, all these residues are found at the active site close to the phosphate binding site. The only mutation which did not result in a significant change of the kinetic parameters was the replacement of Arg63 (Arg54 in the rat enzyme) by Ala (Ostanin *et al.*, 1992). Contrary to conclusions from labelling experiments with the human enzyme (van Etten *et al.*, 1991), this residue is found 18 Å away from the active site at the surface of the protein and is involved in a salt bridge with Glu95 from a neighbouring loop. This salt bridge is probably of structural importance.

Substrate specificity of acid phosphatases

Acid phosphatases have a rather broad substrate specificity. The present structure determination shows that the active site of the enzyme is a rather open cleft with a pocket to bind the phosphate group (Figure 6). This readily accessible active site might be one reason for the broad range of substrates that can be utilized by acid phosphatases. One part of the active site is lined up with the hydrophobic,

predominantly aromatic residues Ile18, Tyr215, Phe171, Trp174, Tyr178, Tyr182, Tyr278, Leu275 and Leu211.

At the opposite side of this cleft, we find two polar residues, Tyr123 and Arg127, which are conserved only in prostatic acid phosphatases. In lysosomal acid phosphatases, these residues are exchanged to Lys and Gly, respectively. Their position at the entrance of the active site surface makes them very probable candidates as responsible for differences in substrate specificity between these two types of phosphatases.

Materials and methods

Enzyme preparation, crystallization and data collection

Recombinant rat prostatic acid phosphatase, produced in Sf9 cells, was prepared and crystallized with PEG as precipitant as described in Vihko *et al.* (1993). Acid phosphatase crystallizes in space group $P3_221$ with cell dimensions $a = b = 89.4$ Å and $c = 152.0$ Å.

Heavy metal derivatives were prepared by soaking crystals with solutions of 5 mM $Pb(CH_3CO_2)_2$ (2 days), 5 mM $SmCl_3$ (1 day) and 1 mM $Hg(CH_3CO_2)_2$ (2 h). Native and derivative data were collected on a Xentronics area detector mounted on a Rigaku rotating anode. Reflexions were measured in 0.1° frames and evaluated with the BUDDHA program (Blum *et al.*, 1989). Data processing was done with the CCP4 suite of programs (Daresbury, UK). Details of data collection are given in Table I.

Phasing

The heavy metal sites could be located by manual inspection of the difference Patterson maps. The correct enantiomorph was established by using the anomalous contribution of the mercury ions in the $Hg(CH_3CO_2)_2$ derivative and was found to be $P3_221$. The space group could also be established from electron density maps calculated for both alternatives. The MIR electron density maps were of good quality and allowed distinction between the two space groups based on the handedness of the α-helices. Based upon the $Hg(CH_3CO_2)_2$ derivative, a common origin for the derivatives was established by cross difference Fourier maps. Although the $SmCl_3$ and $Pb(CH_3CO_2)_2$ derivatives had a common site, all three derivatives, with the anomalous contribution from the mercury derivative, were included in the phase refinement. The final figure of merit after phase refinement was 0.51. Table II summarizes the phasing statistics. The MIR phases were improved by a solvent flattening procedure (Wang, 1985).

Table I. Data collection

Data set	Number of crystals	Resolution (Å)	Measured reflections (% of total)	Unique reflections	R_{merge}[a]
NATI	2	3.0	31216	11240 (79%)	0.053
$Hg(CH_3CO_2)_2$	1	3.0	12806	9522 (67%)	0.066
$Pb(CH_3CO_2)_2$	1	3.0	20292	10723 (75%)	0.041
$SmCl_3$	1	3.0	29028	10449 (73%)	0.073

[a]$R_{merge} = \Sigma\Sigma i \ |I_i - <I>| \ \Sigma|<I>|$ where I_i are the intensity measurements for a reflection and $<I>$ is the mean value for this reflection.

Table II. Phasing statistics

Derivative	Number of sites	R_{deriv}[a]	R_{Cullis}[b]	Phasing power[c]
$Hg(CH_3CO_2)_2$[d]	2	0.241	0.67	2.45
$Pb(CH_3CO_2)_2$	1	0.204	0.89	1.07
$SmCl_3$	1	0.130	0.91	0.75

[a]$R_{deriv} = \Sigma \ |F_{PH} - F_P|/\Sigma|F_P|$ where F_{PH} is the structure factor amplitude of the derivative crystal and F_P is that of the native.
[b]$R_{Cullis} = \Sigma \ ||F_{PH} \pm F_P| - F_H(calc)||/\Sigma|F_{PH} - F_P|$, where F_{PH} and F_P are defined as above and $F_H(calc)$ is the calculated heavy atom structure factor amplitude summed over centric reflections only.
[c]Phasing power: $= F(H)/E$, the r.m.s. heavy atom structure factor amplitudes divided by the lack of closure error.
[d]Anomalous dispersion data included in the refinement.

Model building and refinement

Despite the rather low resolution, the MIR and the solvent flattened maps were of good quality and allowed tracing of most of the polypeptide chain using the graphics program O (Jones *et al.*, 1991). The initial model (325 amino acid residues) was refined using simulated annealing (Brünger, 1989) and the calculated model phases were combined with the MIR phases. After one such round of phase combination, the model could be completed and the amino acid sequence was fitted to the electron density (Roiko *et al.*, 1990). Further refinement with XPLOR led to the present *R*-factor of 20.4% in the resolution interval 8.0−3.0 Å with r.m.s. bond length deviations of 0.021 Å and an r.m.s. deviation from bond angles of 3.9°.

Acknowledgements

References

Bazan,J.F., Fletterick,R.J. and Pilkis,S.J. (1989) *Proc. Natl Acad. Sci. USA*, **86**, 9642−9646.

Blum,M., Metcalf,P., Harrison,S.C. and Wiley,D.C. (1987) *J. Appl. Crystallogr.*, **20**, 235−242.

Bodansky,O. (1972) *Adv. Clin. Chem.*, **15**, 43−147.

Brändén,C.-I. and Jones,T.A. (1990) *Nature*, **343**, 687−690.

Brünger,A. (1989) *Acta Crystallogr.*, **A45**, 50−61.

Campbell,J.W., Watson,H.C. and Hodgson,G.I. (1974) *Nature*, **250**, 301−000.

Jones,T.A., Zou,J.-Y., Cowan,S. and Kjeldgaard,M. (1991) *Acta Crystallogr.*, **A47**, 110−119.

Lin,M.F. and Clinton,G.M. (1986) *Biochem. J.*, **234**, 351−357.

Morris,M.F., Waheed,A., Risley,J.M. and van Etten,R.L. (1989) *Clin. Chim. Acta*, **182**, 9−20.

Ostanin,K., Harms,E.H., Stevis,P.E., Kuciel,R., Zhou,M.-M. and van Etten,R.L. (1992) *J. Biol. Chem.*, **267**, 22830−22836.

Risley,J.M. and van Etten,R.L. (1987) *Arch. Biochem. Biophys.*, **258**, 404−412.

Roiko,K., Jänne,O.A. and Vihko,P. (1990) *Gene*, **89**, 223−229.

Rönnberg,L., Vihko,P., Sajanti,E. and Vihko,R. (1981) *Int. J. Androl.*, **4**, 372−378.

Sowadski,J.M., Handschumacher,M.D., Krishna Murthy,H.M., Foster,B.A. and Wyckoff,H.W. (1985) *J. Mol. Biol.*, **186**, 417−433.

van Etten,R.L. (1982) *Ann. NY Acad. Sci.*, **390**, 27−51.

van Etten,R.L., Davidson,R., Stevis,P., MacArthur,H. and Moore,D. (1991) *J. Biol. Chem.*, **266**, 2313−2319.

Vihko,P., Lukbarinen,O., Kontturi,M. and Vihko,R. (1981) *Cancer Res.*, **41**, 1180−1183.

Vihko,P., Virkkunen,P., Henttu,P., Roiko,K., Solin,T. and Huhtala,M.-L. (1988) *FEBS Lett.*, **236**, 275−281.

Vihko,P., Kurkela,R., Porvari,K., Herrala,A., Lindfors,A., Lindqvist,Y. and Schneider,G. (1992) *Proc. Natl Acad. Sci. USA*, **90**, 799−803.

Vincent,J.B., Crowder,M.W. and Averill,B.A. (1992) *Trends Biochem. Sci.*, **17**, 105−110.

Wang,B.C. (1985) *Methods Enzymol.*, **115**, 90−112.

Winn,S.I., Watson,H.C., Harkins,R.N. and Fothergill,L.A. (1981) *Philos. Trans. R. Soc. Lond.*, **B, 293**, 121−130.

Yam,L.T. (1974) *Am. J. Med.*, **56**, 604−616.